Half-metallicity in graphene nanoribbons with topological line defects

Xianqing Lin and Jun Ni*

Department of Physics and State Key Laboratory of Low-Dimensional Quantum Physics, Tsinghua University, Beijing 100084, People's Republic of China

(Received 7 February 2011; revised manuscript received 21 July 2011; published 11 August 2011)

First-principles calculations have been performed to investigate the electronic properties of graphene nanoribbons with topological line defects composed of octagons and fused pentagons. We find that the edge-passivated zigzag graphene nanoribbons (ZGNRs) with the line defects along the edge show half-metallicity as the line defect is close to one edge. The electronic properties of the ZGNRs with line defects can be tuned by changing the ribbon width and the position of the line defect. When the position of the line defect changes, there are transitions from an antiferromagnetic semiconductor to an antiferromagnetic half-metal, and then to a ferromagnetic metal, suggesting the potential applications of the system in spintronic devices.

DOI: 10.1103/PhysRevB.84.075461 PACS number(s): 73.22.−f, 75.75.−c, 71.55.−i

I. INTRODUCTION

Graphene has been an important two dimensional material for exploring the rich condensed-matter physical phenomena[1–3] and is expected to play an important role in post-silicon electronics.[4] The graphene itself and the quasi-one-dimensional graphene ribbons with widths in the nanometer scale have attracted extensive research.[5–10] Among graphene nanoribbons with various types of edges, zigzag graphene nanoribbons (ZGNRs) have been shown to have nonzero and direct band gaps with ferromagnetically ordered edge states at each edge having opposite spin orientation.[11] In particular, half-metallicity has been realized in ZGNRs in many ways.[12–15] When a transverse electric field is applied across the edges of the nanoribbons, ZGNRs are predicted to exhibit half-metallicity using the density functional theory (DFT) within both the local spin density approximation (LSDA)[12] and generalized gradient approximation (GGA).[13] DFT calculations have also shown that when a certain number of zigzag carbon chains in the middle of ZGNRs are replaced with zigzag boron-nitrogen chains, the nanoribbons exhibit semiconducting and half-metallic behavior,[14] which suggests that the extended chemical doping is a way of establishing half-metallicity in zigzag nanoribbons. The external electric field can also regulate the electronic structures of these modified nanoribbons.[14,16] In addition, DFT calculations show that the armchair nanotubes obtained by replacing a certain number of zigzag carbon chains with zigzag boron-nitrogen chains can have half-metallicity.[17]

Some of the ZGNRs with divacancies or divacancies combined with Stone-Wales-like defects have been proposed to have spin polarization higher than 90% in the transmittance,[18] which implies that the introduction of the topological defects can be one way of establishing half-metallicity in ZGNRs. However, the presence of the topological point defects can only make ZGNRs close to half-metals. Recently, topological line defects composed of octagons and fused pentagons has been observed experimentally in graphene sheets.[19] The two domains of the graphene sheet separated by the line defect both have the zigzag crystallographic direction along the line defect. The presence of the line defect makes the graphene sheet show the metallic character,[19] which is consistent with the theory proposed by Yazyev *et al.* based on the momentum conservation rule[20] and is confirmed by first-principles calculations by Okada *et al.*[21] Scanning tunneling microscope (STM) measurements of graphene sheets with line defects show that states around the Fermi level are mainly distributed in the line defect and decay away from the line defect.[19] Such electronic states localized in the line defect have also been observed in the armchair carbon nanotubes with line defects based on first-principles calculations.[22] The armchair nanotubes with line defects show ferromagnetic spin ordering along the tube axis and remain metallic for all tube diameters.[22] Because the spin polarization at the two edges of ZGNRs can have opposite orientation, when the line defect is introduced into ZGNRs, the presence of localized states in the line defect may have different effects on the electronic states of the two spins and change the magnetic behavior of the system. Therefore, it is important to investigate the effects of the line defect on the electronic properties of ZGNRs and the possibility of realizing half-metallicity in ZGNRs by the introduction of the line defect. In this paper, we show that the ZGNRs with line defects (LD-ZGNRs) exhibit a rich variety of electronic properties that vary with the ribbon width and the position of the line defect. In particular, we find that LD-ZGNRs with certain ribbon widths show half-metallicity as the line defect is close to one edge.

The outline of this paper is as follows: Section II describes the calculation details. In Sec. III, we show the geometry of LD-ZGNRs and discuss the energetics, spin configuration, and electronic band structures of the system. Section IV is the summary.

II. METHODS

The spin-polarized DFT is employed in our electronic structure calculations using the SIESTA code.[23] The generalized gradient approximation (GGA) with the Perdew-Burke-Ernzerhof exchange-correlation functional[24] is adopted with the norm-conserving pseudopotentials using the Troullier-Martins parametrization[25] and the double zeta basis set plus polarization orbitals. A plane-wave cutoff of 400 Ry for the real space grid is used and the 1D Brillouin zone sampling is done using a $1 \times 1 \times 32$ Monkhorst-Pack grid for the relaxation calculations and a $1 \times 1 \times 96$ Monkhorst-Pack

 ©2011 American Physical Society

grid for the static calculations. The vacuums between edges and between planes in the adjacent unit cells are larger than 20 Å. The tolerance for the energy convergence is 10^{-5} eV. All the structures are fully relaxed until the force on each atom is smaller than 0.01 eV/Å. The calculations are verified by VASP[26] using the plane-wave basis set within the generalized gradient approximation. The results of calculations by the two codes are consistent with each other.

III. RESULTS

A. Geometry and energetics of the system

The line defect in a LD-ZGNR consists of one octagon and a pair of pentagons periodically repeated along the edge direction, as shown in Fig. 1. In a graphene sheet, this type of line defect can be formed by translating the two half-lattices relative to each other by a C-C bond length along the armchair direction.[19] The single-layer graphene sheets with such line defects have been obtained on the Ni (111) substrate by Lahiri *et al.* recently.[19] A recent molecular dynamics simulation has also shown that such line defects can be formed spontaneously from defects in the graphene sheet at a high temperature.[21] These graphene sheets containing line defects can be transferred to other substrates for postprocessing.[19] The graphene nanoribbons can be cut from graphene sheets by e-beam lithography,[27] scanning tunneling lithography (STL),[28] atomic force microscope lithography,[29] or chemical reactions with crystallographic selectivity.[30] Among these patterning methods, STL is a promising method of realizing the simultaneous control of the crystallographic orientation and of the ribbon width with high precision.[28,31] For graphene sheets with line defects, the direction of the line defect indicates the zigzag crystallographic orientation for the STL. The atomic structures of the obtained LD-ZGNRs can also be measured with the high-resolution STM. In a LD-ZGNR, on each side of the line defect, there is a ribbon with zigzag carbon chains. We refer to the two ribbons as the left and right ribbons,

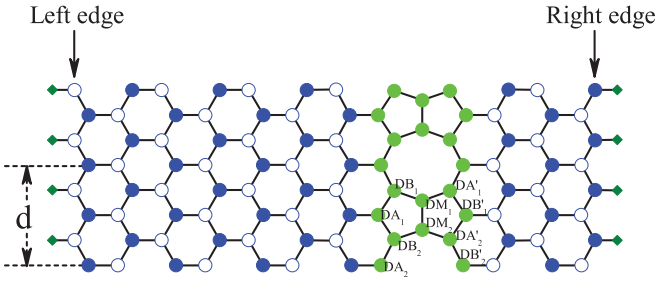

FIG. 1. (Color online) The relaxed structure of 7-3-LD-ZGNR. The circles represent carbon atoms and the rhombuses represent hydrogen atoms. The carbon atoms in the line defect are represented by the filled gray circles. The sublattice A and B of the left and right ribbons are represented by the empty circles and filled black circles, respectively. The structure is periodic along the line defect with a lattice constant denoted as d. The atoms in the middle of the fused pentagons are labeled as DM_1 and DM_2. The atoms in the line defect connected to the left ribbon are labeled as DA_1 and DA_2. The atoms in the line defect connected to DA atoms are labeled as DB_1 and DB_2. The four atoms connected to the the right ribbon are labeled as DA'_1, DB'_1, DA'_2, and DB'_2.

respectively. The widths of the left and right ribbons are defined by the numbers of the zigzag chains denoted as N_1 and N_2 for the left and right ribbons, respectively. We denote the LD-ZGNR with N_1 and N_2 zigzag chains on the left and right sides of the line defect as N_1-N_2-LD-ZGNR. The N_1-N_2-LD-ZGNRs with the same sum of N_1 and N_2 ($N_1 + N_2$) have the same widths. Since N_1-N_2-LD-ZGNR and N_2-N_1-LD-ZGNR have the same structure, we consider the case of $N_1 \geqslant N_2$ only. Figure 1 shows the relaxed structure of 7-3-LD-ZGNR. The structure is periodic along the line defect with a lattice constant d of 4.9 Å. Our relaxation calculations show that all LD-ZGNRs considered in this work have the same lattice constant of 4.9 Å. In the left ribbon, the sublattice that the atoms at the left edge belong to is denoted as the sublattice A and the other one is denoted as the sublattice B. The lattice that the atoms at the right edge belong to is denoted as the sublattice B of the right ribbon, and the other sublattice of the right ribbon is denoted as the sublattice A. The two atoms in the middle of the fused pentagons are labeled as DM_1 and DM_2. In the line defect, the four atoms on the left side of the two DM atoms are labeled as DB_1, DA_1, DB_2, and DA_2, and the four atoms connected to the right ribbon are labeled as DA'_1, DB'_1, DA'_2, and DB'_2, as shown in Fig. 1.

To investigate the stabilities of the system, we have calculated the total energies of the N_1-N_2-LD-ZGNRs with the same width. The results of calculations show that the stability of the LD-ZGNRs with the same width varies as a function of the position of the line defect. For a given $N_1 + N_2$ ($N_1 \geqslant N_2$, as noted above), the total energy per unit cell of the LD-ZGNR decreases as the the line defect approaches the right edge. Hence, when N_2 is equal to zero, the LD-ZGNR with a specific width has the lowest total energy. However, the difference in the energy per unit cell between the structures with the same width but different defect positions is quite small. For example, for the LD-ZGNRs with $N_1 + N_2 = 10$, the total energy per unit cell of the structure with $N_1 = 9$ ($N_2 = 1$) is lower than that for $N_1 = 5$ ($N_2 = 5$) by 0.08 eV. The difference in the total energy per unit cell between the structure with $N_1 = 9$ ($N_2 = 1$) and that with $N_1 = 10$ ($N_2 = 0$) is 0.28 eV, and the energy difference per atom is only 5.2 meV.

As to the stability of the line defect, we note that the STM measurements of the line defects in graphene sheets by Lahiri *et al.* were performed at room temperature and the STM images show that the line defect remains straight and atomically precise.[19] The molecular dynamics simulation by Okada *et al.* has also shown that the line defect in a graphene sheet remains stable at a significantly high temperature.[21] Recently, grain boundaries in single-layer graphene sheets have been observed and are demonstrated to be stable at room temperature.[32] In addition, there have been several theoretical studies that have investigated the electronic structures of these extended topological defects including the line defect and grain boundaries.[20,33,34] Since the graphene nanoribbons with line defects are strongly bonded carbon networks as the graphene sheets with line defects, the line defect in a graphene nanoribbon is thus also stable at room temperature. To confirm this point, we have calculated the energies of the structures with the migration or evaporation of one atom or C-C cluster in the middle of the line defect (see Fig. 1 for the structure of the line defect and the two DM_1 and DM_2

atoms are defined to be a C-C cluster). We use the supercell consisting of three unit cells of the 5-1-LD-ZGNR along the line defect. For the migration of an atom in the middle of the line defect, we consider placing the DM_1 atom on the top of the DB_1, DA_1', and DM_2 atoms (top sites) and on the top of the DB_1-DA_1', DB_1-DM_2, and DA_1'-DM_2 lines as well as the C-C bonds (bridge sites) near the original DM_1 atom. Most of the structures relax into the pristine LD-ZGNR except for the bridge sites of the DM_2-DB_2 and DM_2-DA_2' bonds and the top site of the DM_2 atom. The energy of the relaxed structure when placing the DM_1 atom on the top of the DM_2 atom, the DM_2-DB_2 bond or the DM_2-DA_2' bond is 6.2 eV higher than the energy of the pristine LD-ZGNR. For the migration of a C-C cluster in the line defect, we have considered rotating the DM_1-DM_2 bond around the DA_1'-DA_2' line. When the plane containing the DM_1, DM_2, DA_1', and DA_2' atoms is almost perpendicular to the plane of the nanoribbon, the energy of the relaxed structure is 9.0 eV higher than that of the pristine LD-ZGNR. For the evaporation of an atom or a C-C cluster, we consider the structures with the DM_1 atom or DM_1-DM_2 cluster missing in the middle of the line defect. We find that energies of 16.1 eV and 12.3 eV are required for the DM_1 atom and DM_1-DM_2 cluster to break out of the line defect, respectively. Therefore, the energy barrier for the migration or evaporation of atoms in the middle of the line defect in a LD-ZGNR is extremely high. The line defect in a LD-ZGNR is thus stable at room temperature.

B. Spin configuration of the ground state

The ground state of the pristine ZGNRs prefers the antiferromagnetic spin configuration with the opposite spin polarizations at the two edges. The energy difference between the ferromagnetic (FM) and antiferromagnetic (AFM) spin configurations decreases and eventually vanishes as the width increases beyond the decay length of the spin polarization at the two edges.[35,36] However, our calculations show that for the N_1-N_2-LD-ZGNRs with a specific $N_2 > 0$, when N_1 is significantly larger than N_2, the ground state prefers the FM configuration, while for small N_1 it remains antiferromagnetic. In the case of $N_2 = 1$, the ground state has the FM configuration for $N_1 \geqslant 11$ and is antiferromagnetic when N_1 is in the range of 1 to 10. When $N_2 = 2$, the ground state remains antiferromagnetic until N_1 increases beyond 17. If $N_2 = 0$, because there are no zigzag carbon chains on the right side of the line defect, the spin polarization at the right edge is much weaker than that at the left edge. For example, for 10-0-LD-ZGNR, the magnetic moment per atom is 0.28 μ_B at the left edge and is only 0.02 μ_B at the right edge.

For the pristine ZGNRs in the AFM (FM) state, the contributions of the left and right edges to the spin density at each inner site of the nanoribbons have the same (opposite) orientation. The amplitude of the spin density at each inner site in the AFM state is thus larger than that in the FM state. Therefore, the exchange energy gain due to the spin polarization of the nanoribbon in the AFM state is larger than that in the FM state. This explains that the energies of the pristine ZGNRs in the AFM state are lower than those in the FM state.[35] For LD-ZGNRs, the presence of the line defect affects the constructive contribution of the AFM spin

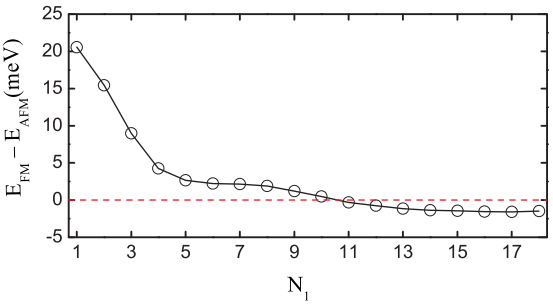

FIG. 2. (Color online) The energy difference $E_{FM} - E_{AFM}$ per unit cell for N_1-1-LD-ZGNRs between the FM and AFM configurations as a function of N_1. The dashed line represents the zero energy difference.

configuration to the spin density of the nanoribbons. As a result, the ground state becomes ferromagnetic when N_1 is significantly larger than N_2. We consider the case of $N_2 = 1$ for a detailed analysis. Figure 2 shows the energy difference $E_{FM} - E_{AFM}$ per unit cell between the FM and AFM configurations of N_1-1-LD-ZGNRs as a function of N_1. Similar to the pristine ZGNRs, the energy difference decreases as N_1 increases. For $N_1 = 7$ with the width of 2.1 nm, the energy difference is 2.3 meV, while the pristine ZGNR with a width close to that of 7-1-LD-ZGNR has a larger energy difference of about 5 meV[36]. The decrease in the energy difference from the pristine ZGNR to the LD-ZGNR is attributed to the presence of the line defect in the LD-ZGNR. In contrast to the pristine ZGNRs, when N_1 reaches 11 with the width of 3.0 nm, the energy difference for N_1-1-LD-ZGNRs becomes negative. Thus the FM state is more stable than the AFM state for $N_1 \geqslant 11$ with $N_2 = 1$.

We define the spin polarization at the left edge of LD-ZGNRs as spin-up. Then, in the AFM and FM states, the right edge has spin-down and spin-up polarizations, respectively. For 5-1-LD-ZGNR, the ground state is antiferromagnetic. We denote the density of spin-up and spin-down electrons as ρ_{up} and ρ_{down}, respectively. The spin density $\rho_{up} - \rho_{down}$ for 5-1-LD-ZGNR with the density integrated in the direction perpendicular to the ribbon plane for the AFM and FM states is shown in Figs. 3(a) and 3(b). Figure 3(c) shows the spin density difference between the AFM state and the FM state $|\rho|_{AFM} - |\rho|_{FM}$ integrated in the unit cell within the plane perpendicular to the armchair direction. The ground state of 13-1-LD-ZGNR has the FM configuration. Figure 4 shows the spin density for 13-1-LD-ZGNR. As shown in Fig. 4(a), the left edge is quite far away from the line defect for 13-1-LD-ZGNR. The spin density in the right part of the nanoribbon is thus primarily contributed by the spin polarization at the right edge. As shown in Figs. 4(a) and 4(b), the spin density in the left pentagons of the line defect (the DA_1, DB_1, DB_2, DM_1, and DM_2 sites) and the sublattice A of the left ribbon near the line defect has the same orientation as that at the right edge for both the AFM and FM states. For other LD-ZGNRs, considering only the spin polarization at the right edge with the initial guess for the magnetic moment at each site set to zero except the sites at the right edge in static calculations, our calculations show that the contribution of the spin polarization at the right edge to the spin density in the left pentagons and the sublattice

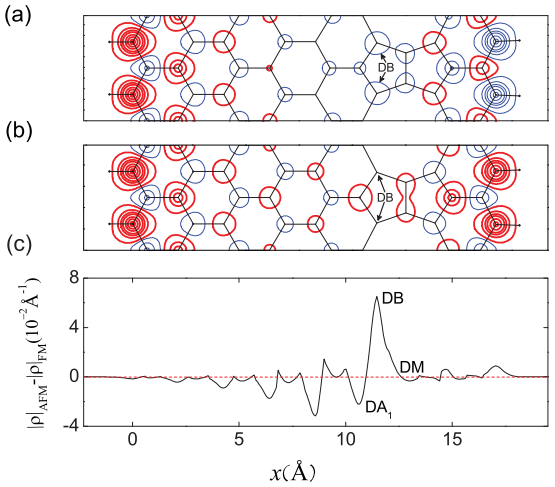

FIG. 3. (Color online) Contour plots for the spin density $\rho_{up} - \rho_{down}$ of 5-1-LD-ZGNR in the (a) AFM and (b) FM states. The thicker lines indicate the spin-up density with $\rho_{up} - \rho_{down} > 0$. The range of isovalues is [0.01,0.40] Å^{-2} in both (a) and (b). The thinner lines represent the spin-down density with $\rho_{up} - \rho_{down} < 0$. The range of isovalues is [−0.32, − 0.01] Å^{-2} in (a) and [−0.1, − 0.01] Å^{-2} in (b). (c) The difference between the absolute values of the spin density of the AFM state and the FM state $|\rho|_{AFM} - |\rho|_{FM}$ with $|\rho| = |\rho_{up} - \rho_{down}|$ integrated within the plane perpendicular to the armchair direction. x is the coordinate along the width of the nanoribbon with the left edge atoms located at $x = 0$.

A of the left ribbon has the same orientation as that at the right edge. On the other hand, when we consider only the spin polarization at the left edge, the calculations show that the spin density in the sublattice A of the left ribbon and at the DA_1 site has the same orientation as that at the left edge, while in the sublattice B of the left ribbon and at the DB sites, the orientation of the spin density is opposite with respect to that at the left edge.

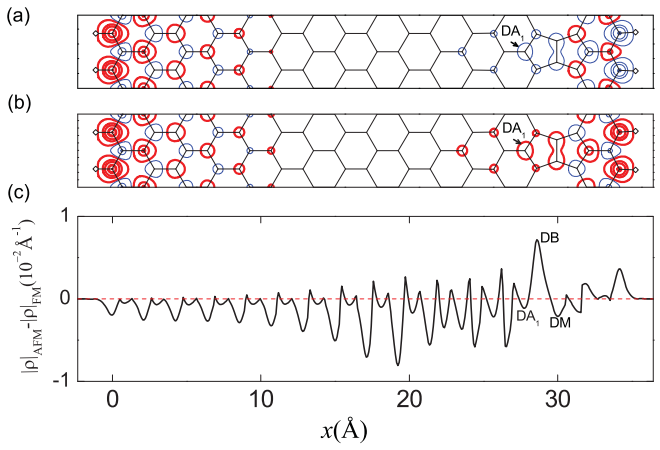

FIG. 4. (Color online) Contour plots for the spin density $\rho_{up} - \rho_{down}$ of 13-1-LD-ZGNR in the (a) AFM and (b) FM states. The thicker lines indicate the spin-up density with $\rho_{up} - \rho_{down} > 0$. The range of isovalues is [0.01,0.43] Å^{-2} in both (a) and (b). The thinner lines represent the spin-down density with $\rho_{up} - \rho_{down} < 0$. The range of isovalues is [−0.31, − 0.01] Å^{-2} in (a) and [−0.1, − 0.01] Å^{-2} in (b). (c) $|\rho|_{AFM} - |\rho|_{FM}$ as a function of x.

For LD-ZGNRs, as shown in Figs. 3(c) and 4(c), the amplitude of the spin density in the line defect and the right ribbon in the AFM state is larger than that in the FM state. The exchange energy contributed by the spin density at the sites in the line defect and the right ribbon in the AFM state is thus lower than that in the FM state. Then, these sites have a positive contribution to the energy difference $E_{FM} - E_{AFM}$. In the left ribbon of LD-ZGNRs, the amplitude of the spin density in the AFM state is, however, smaller than that in the FM state. Thus the left ribbon contributes negatively to $E_{FM} - E_{AFM}$. The reasons for lower exchange energy due to larger amplitude of spin density are explained as follows. For LD-ZGNRs, our calculations show that the AFM and FM states have almost the same total electron density $\rho_{up} + \rho_{down}$. For example, the amplitude of the difference in the $\rho_{up} + \rho_{down}$ of the AFM and FM states, which is integrated in the unit cell within the plane perpendicular to the armchair direction, is smaller than 0.0085 Å^{-1} for 5-1-LD-ZGNR and smaller than 0.0015 Å^{-1} for 13-1-LD-ZGNR. Within the LSDA framework, the exchange energy per electron is[37]

$$\varepsilon_X(\rho_{up},\rho_{down}) = -\frac{3}{8}\left(\frac{3}{\pi}\right)^{1/3}(\rho_{up}+\rho_{down})^{1/3} \times [(1+\zeta)^{4/3} + (1-\zeta)^{4/3}]$$

in atomic units, where $\zeta = |\rho_{up} - \rho_{down}|/(\rho_{up} + \rho_{down})$ is the amplitude of the relative spin polarization. For a specific $\rho_{up} + \rho_{down}$, ε_X monotonically decreases as ζ varies from 0 to 1. Taking into account the density gradient correction within the GGA framework, ε_X is still a decreasing function of ζ for the specific total electron density and density gradient.[24] As shown in Figs. 3(c) and 4(c), in the line defect and the right ribbon, $|\rho_{up} - \rho_{down}|$ in the AFM state $|\rho|_{AFM}$ is larger than that in the FM state $|\rho|_{FM}$. That is, the AFM state has larger ζ than the FM state in this region. Then, ε_X in this region in the AFM state is lower than that in the FM state. Therefore, the total exchange energy contributed by the line defect and the right ribbon in the AFM state is lower than that in the FM state. In the left ribbon of LD-ZGNRs, the amplitude of the relative spin polarization ζ in the AFM state is smaller than that in the FM state. ε_X in the left ribbon in the AFM state is thus higher than that in the FM state, making the total exchange energy contributed by the left ribbon in the AFM state higher than that in the FM state.

In the line defect and the right ribbon of LD-ZGNRs, the positive $|\rho|_{AFM} - |\rho|_{FM}$ is primarily contributed by the DB sites, as shown in Figs. 3(c) and 4(c). In the AFM state, both the left and right edges contribute to the spin-down density at the DB sites. The spin polarization is enhanced at these sites. Whereas the FM state contributes destructively to the spin density at the DB sites. Therefore, $|\rho|_{AFM} > |\rho|_{FM}$ at the DB sites. In the left ribbon, the spin-up polarization at the left edge has a spin-up contribution to the spin density in the sublattice A and a spin-down contribution in the sublattice B. The contribution of the spin polarization at the right edge to the spin density in the sublattice A of the left ribbon has the same orientation as that at the right edge. In the AFM and FM states, the right edge has thus a contribution of spin-down and spin-up density in the sublattice A, respectively, as shown in Fig 4(a) and 4(b) for 13-1-LD-ZGNR. The contribution of

the right edge to the spin density in the sublattice B of the left ribbon is very small. Therefore, in the FM state, the left and right edges contribute constructively to the spin density in the sublattice A. However, in the AFM state, the contributions of the left and right edges to the spin density in the sublattice A are destructive. As a result, $|\rho|_{\mathrm{AFM}} < |\rho|_{\mathrm{FM}}$ in the sublattice A of the left ribbon, as shown in Figs. 3(c) and 4(c).

For N_1-1-LD-ZGNRs, the amplitude of $|\rho|_{\mathrm{AFM}} - |\rho|_{\mathrm{FM}}$ in the line defect and the right ribbon decreases as N_1 increases, as shown in Figs. 3(c) and 4(c). Therefore, the positive contribution of the line defect and the right ribbon to $\mathrm{E_{FM}}-\mathrm{E_{AFM}}$ decreases with the increase of N_1. When N_1 increases from 5 to 13, $|\rho|_{\mathrm{AFM}} - |\rho|_{\mathrm{FM}}$ decreases from 6.5 to 0.7 $\mathrm{Å}^{-1}$ at the DB sites and $\mathrm{E_{FM}} - \mathrm{E_{AFM}}$ decreases from 2.7 to -1.2 meV.

C. Electronic band structures

LD-ZGNRs with the FM ground state are metallic. This is similar to the pristine ZGNRs in the FM state[36] and is consistent with the results of calculations by Okada *et al.* for a LD-ZGNR in the FM state.[21] When $N_2 = 0$, N_1-0-LD-ZGNRs also show metallic behavior. LD-ZGNRs with the AFM ground state show semiconducting or half-metallic behavior. For half-metallic LD-ZGNRs, the spin-up state is metallic while the spin-down state shows semiconducting behavior. In the following, we will consider the electronic band structures of LD-ZGNRs with the AFM ground state.

We first consider the systems with $N_1 + N_2 = 10$. Under the condition $N_1 \geqslant N_2$, N_1 can be 5, 6, 7, 8, or 9. The corresponding N_2 is 5, 4, 3, 2, or 1, respectively. The spin-down channel of the five structures is semiconducting, while the spin-up channel shows semiconducting or metallic behavior. We denote the band gap of the spin-down state as Δ_{down}. For the semiconducting spin-up state, the band gap is denoted as Δ_{up}. When the spin-up state is metallic, Δ_{up} represents the difference in the eigenvalues of the lowest conduction band and the highest valence band of the spin-up state. Δ_{down} and Δ_{up} are shown as a function of N_1 in Fig. 5(d). Figures 5(a), 5(b), and 5(c) show the band structures for $N_1 = 5$, 7, and 9, respectively. For $N_1 = 5$, the spin-up and spin-down bands are degenerate. The band gap is 0.14 eV. The band gap of the pristine ZGNR with similar width is about 0.23 eV within the LSDA calculations.[11] When N_1 increases from 5 to 9, Δ_{down} increases from 0.14 eV to 0.24 eV, whereas Δ_{up} decreases from 0.14 eV to –0.10 eV. The negative Δ_{up} for $N_1 = 9$ means that the valence band and the conduction band overlap so that a hole channel near $kd = \pi$ (the X point) and an electron channel near $kd = 0.42\pi$ appear at the Fermi level E_F. On the other hand, the spin-down state is semiconducting with a band gap of 0.24 eV for $N_1 = 9$. Thus, 9-1-LD-ZGNR exhibits half-metallic behavior. In addition, we note that the band gaps of the spin-down state and the semiconducting spin-up state of the N_1-N_2-LD-ZGNRs with $N_1 + N_2 = 10$ are all indirect. For the semiconducting spin-up state, the highest valence band remains at the X point and the lowest conduction band moves away from the Γ point as N_1 increases. For the spin-down state, with the increase of N_1, the highest valence band and the lowest conduction band move away from the X point and the Γ point, respectively.

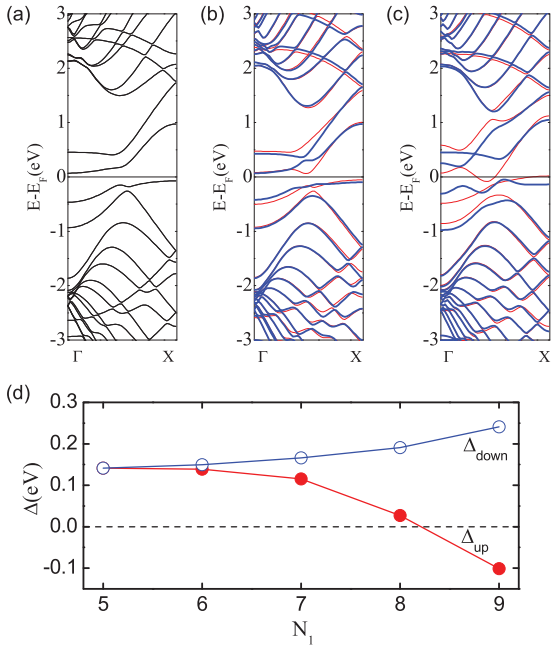

FIG. 5. (Color online) (a), (b), and (c) The spin resolved band structures of LD-ZGNRs for $N_1 = 5$, 7, and 9 with $N_1 + N_2 = 10$. The thinner and thicker lines denote bands of spin-up and spin-down, respectively. (d) The band gap of the spin-down state Δ_{down} and the eigenvalue difference Δ_{up} between the lowest conduction band and the highest valence band of the spin-up state as a function of N_1.

We next consider the systems with $N_2 = 1$. We find that N_1-1-LD-ZGNRs exhibit half-metallicity when N_1 is in the range of 5 to 10 with the width from 1.7 to 3.0 nm, while N_1-1-LD-ZGNRs with N_1 in the range of $1 \sim 4$ show semiconducting behavior for both spins. As shown in Fig. 6(d), Δ_{up} decreases from 0.32 eV to 0.01 eV as N_1 increases from 1 to 4. When $N_1 \geqslant 5$, Δ_{up} becomes negative, namely, the spin-up state shows metallic behavior. Δ_{down} remains in the range of $0.22 \sim 0.32$ eV as N_1 increases from 1 to 10. For half-metallic N_1-1-LD-ZGNRs, Δ_{down} is in the range of $0.22 \sim 0.31$ eV. In comparison, the pristine ZGNR with a width of 2.2 nm has a band gap of $0.3 \sim 0.4$ eV for the semiconducting spin state when it shows half-metallicity under a transverse electric field.[12]

The band structures for $N_1 = 3$, 5, and 7 ($N_2 = 1$) are shown in Figs. 6(a), 6(b), and 6(c), respectively. The transition from a semiconductor to a half-metal for the N_1-1-LD-ZGNRs with the increase of N_1 is reflected in the variation of the difference Δ_X in the eigenvalues of the spin-up and spin-down valence states at the X point as a function of N_1, as shown in Fig. 6(d). For $N_1 = 1 \sim 10$, Δ_X remains positive and increases as N_1 increases. When Δ_X reaches 0.11 eV ($N_1 = 5$), the valence band and the conduction band of the spin-up state overlap with each other, resulting in half-metallicity in the system. We denote the valence eigenfunction of the σ ($\sigma =$ up or down) spin at the X point as $\psi^{\sigma}_{v,X}$. $|\psi^{\sigma}_{v,X}|^2$ has the same spatial distribution for both spins. Figures 7(a) and 7(b) show the distribution of $|\psi^{\sigma}_{v,X}|^2$ for $N_1 = 3$ and 7, respectively. In the line defect, $|\psi^{\sigma}_{v,X}|^2$ is distributed at the $\mathrm{DM_1}$, $\mathrm{DM_2}$, $\mathrm{DA_1}$, and $\mathrm{DB_1'}$ sites. In the left ribbon, $|\psi^{\sigma}_{v,X}|^2$ is distributed in the

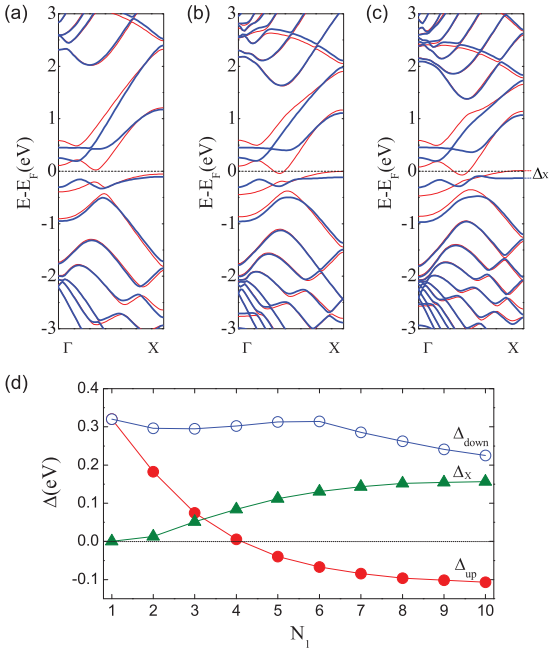

FIG. 6. (Color online) (a), (b), and (c) The spin resolved band structures of LD-ZGNRs for $N_1 = 3$, 5, and 7 with $N_2 = 1$. (d) $\Delta_{\rm up}$, $\Delta_{\rm down}$ and the eigenvalue difference Δ_X between the spin-up and spin-down valence states at the X point as a function of N_1.

sublattice A. In the right ribbon, $|\psi^{\sigma}_{v,X}|^2$ is distributed in the the sublattice B. For the LD-ZGNRs with the AFM ground state, the DM_1, DM_2, DB'_1 sites and the sublattice B of the right ribbon have spin-down density, as shown in Fig. 4(a). Then, $\rho_{\rm up} < \rho_{\rm down}$ at these sites. Since the exchange potential $V^{\sigma}_x \propto -(\rho_\sigma)^{1/3}$,[38] the exchange energy of the spin-up valence state $\psi^{\rm up}_{v,X}$ contributed by these sites is higher than that for the spin-down state $\psi^{\rm down}_{v,X}$. These sites thus have a positive contribution to the eigenvalue difference between the spin-up and spin-down state Δ_X. For $N_1 = 2$ and 3, $\rho_{\rm up} > \rho_{\rm down}$ at the DA_1 site. The contribution of the DA_1 site to Δ_X is negative. When $N_1 \geqslant 4$, $\rho_{\rm up}$ becomes smaller than $\rho_{\rm down}$, the DA_1 site has a positive contribution to Δ_X. In the left ribbon, $|\psi^{\sigma}_{v,X}|^2$ is distributed at the sites in the sublattice A, which are close to the line defect, as shown in Fig. 7. At these sites, $\rho_{\rm up} > \rho_{\rm down}$, as shown in Fig. 3(a). Thus the contribution of these sites to Δ_X is negative. Because the spin polarization in the

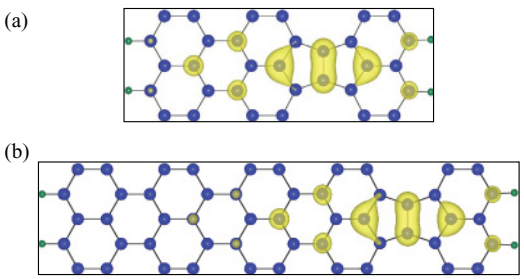

FIG. 7. (Color online) The spatial distribution of the valence eigenfunction at the Xpoint for (a) 3-1-LD-ZGNR and (b) 7-1-LD-ZGNR. The isosurface is 0.015 $Å^{-3}$.

sublattice A of the left ribbon where $|\psi^{\sigma}_{v,X}|^2$ is distributed is much weaker than that in the line defect and in the right ribbon, as shown in Figs. 3(a) and 4(a), the amplitude of the negative contribution of the left ribbon to Δ_X is smaller than that of the positive contribution of the line defect and the right ribbon to Δ_X. Then, $\Delta_X \geqslant 0$ for $N_1 \geqslant 1$ with $N_2 = 1$. When N_1 increases from 1 to 10, the sites in the left ribbon where $|\psi^{\sigma}_{v,X}|^2$ is distributed move away from the left edge, as shown in Figs. 7(a) and 7(b), leading to weaker spin-polarization in these sites so that the amplitude of the negative contribution of the left ribbon to Δ_X decreases. Moreover, with the increase in the width of the left ribbon, the spin polarization in the line defect and the right ribbon becomes stronger, making the positive contribution of the line defect and the right ribbon to Δ_X increase. Therefore, Δ_X increases with the increase of N_1, which leads to half-metallicity in the system. When $N_1 \geqslant 5$ with $\Delta_X \geqslant 0.11$ eV, the valence band and the conduction band of the spin-up state overlap with each other so that a hole channel near the X point appears at E_F. In comparison, when the pristine ZGNRs under a transverse electric field become half-metallic, it is the electron channel that appears near the X point at E_F, with the states of the gap-narrowing spin of the conduction band near the X point localized at one edge of the nanoribbon.[12]

Our calculations show that for a specific and small N_2, there is a critical N_1 for achieving half-metallicity in N_1-N_2-LD-ZGNRs. The critical value of N_1 increases as N_2 increases. When $N_2 = 1$, the system becomes half-metallic when $N_1 = 5$. While for $N_2 = 2$, the critical N_1 for achieving half-metallicity in N_1-2-LD-ZGNRs is 14.

IV. SUMMARY

Our spin polarized GGA calculations show that the zigzag graphene nanoribbons N_1-N_2-LD-ZGNRs with topological line defects have the antiferromagnetic or ferromagnetic ground state. For a small number N_2 of zigzag chains in the right ribbon, LD-ZGNRs with the antiferromagnetic ground state exhibit half-metallic behavior when the number N_1 of zigzag chains in the left ribbon is much larger than N_2. For the LD-ZGNRs with $N_2 = 1$, the ground state prefers the antiferromagnetic spin configuration with the opposite spin polarization at the two edges when N_1 is in the range of 1 to 10. For $N_1 > 10$, spin polarizations at the two edges have the same orientation and the ground state becomes ferromagnetic. The presence of the line defect weakens the constructive contribution of the antiferromagnetic spin configuration to the spin polarization of ZGNRs, making the ground state ferromagnetic when N_1 is significantly larger than N_2. The LD-ZGNRs with the ferromagnetic ground state are metallic. For $N_2 = 1$, N_1-1-LD-ZGNRs with N_1 in the range of $1 \sim 4$ show semiconducting behavior for both spins, while the system exhibits half-metallicity when N_1 is in the range of 5 to 10 with the band gap of the semiconducting spin state in the range of $0.22 \sim 0.31$ eV. The transition from a semiconductor to a half-metal as N_1 increases can be attributed to the fact that the valence eigenfunctions at the X point for both spins are distributed in and near the line defect where primarily the spin-down density is distributed. In the case of $N_2 = 2$, LD-ZGNRs exhibit half-metallic behavior for $N_1 = 14 \sim 17$. In

addition, the total energy per unit cell of the nanoribbons with a specific width decreases as the line defect approaches one edge. Because of the rich electronic and magnetic properties, the zigzag graphene nanoribbons with topological line defects may have potential applications in spintronic devices.

ACKNOWLEDGMENTS

This research was supported by the National Natural Science Foundation of China under Grant Nos. 10974107 and 10721404.

*junni@mail.tsinghua.edu.cn

[1] A. K. Geim and K. S. Novoselov, Nature Mater. **6**, 183 (2007).
[2] A. H. Castro Neto, F. Guinea, N. M. R. Peres, K. S. Novoselov, and A. K. Geim, Rev. Mod. Phys. **81**, 109 (2009).
[3] D. S. L. Abergel, V. Apalkov, J. Berashevich, K. Ziegler, and T. Chakraborty, Adv. Phys. **59**, 261 (2010).
[4] F. Schwierz, Nature Nanotech. **5**, 487 (2010).
[5] K. S. Subrahmanyam, A. K. Manna, S. K. Pati, and C. N. R. Rao, Chem. Phys. Lett. **497**, 70 (2010).
[6] A. K. Manna and S. K. Pati, Chem. Asian J. **4**, 855 (2009).
[7] K. Wakabayashi, M. Fujita, H. Ajiki, and M. Sigrist, Phys. Rev. B **59**, 8271 (1999).
[8] S. Dutta, S. Lakshmi, and S. K. Pati, Phys. Rev. B **77**, 073412 (2008).
[9] S. Dutta and S. K. Pati, Carbon **48**, 4409 (2010).
[10] S. Dutta and S. K. Pati, J. Mater. Chem. **20**, 8207 (2010).
[11] Y.-W. Son, M. L. Cohen, and S. G. Louie, Phys. Rev. Lett. **97**, 216803 (2006).
[12] Y.-W. Son, M. L. Cohen, and S. G. Louie, Nature (London) **444**, 347 (2006).
[13] S. Dutta and S. K. Pati, J. Phys. Chem. B **112**, 1333 (2008).
[14] S. Dutta, A. K. Manna, and S. K. Pati, Phys. Rev. Lett. **102**, 096601 (2009).
[15] E.-J. Kan, Z. Li, J. Yang, and J. G. Hou, J. Am. Chem. Soc. **130**, 4224 (2008).
[16] Z. Zhang and W. Guo, Phys. Rev. B **77**, 075403 (2008).
[17] B. Huang, C. Si, H. Lee, L. Zhao, J. Wu, B.-L. Gu, and W. Duan, Appl. Phys. Lett. **97**, 043115 (2010).
[18] R. Y. Oeiras, F. M. Araújo-Moreira, and E. Z. da Silva, Phys. Rev. B **80**, 073405 (2009).
[19] J. Lahiri, Y. Lin, P. Bozkurt, I. I. Oleynik, and M. Batzill, Nature Nanotech. **5**, 326 (2010).
[20] O. V. Yazyev and S. G. Louie, Nature Mater. **9**, 806 (2010).
[21] S. Okada, T. Kawai, and K. Nakada, J. Phys. Soc. Jpn. **80**, 013709 (2011).
[22] S. Okada, K. Nakada, K. Kuwabara, K. Daigoku, and T. Kawai, Phys. Rev. B **74**, 121412(R) (2006).
[23] J. M. Soler, E. Artacho, J. D. Gale, A. García, J. Junquera, P. Ordejón, and D. Sánchez-Portal, J. Phys.: Condens. Matter. **14**, 2745 (2002).
[24] J. P. Perdew, K. Burke, and M. Ernzerhof, Phys. Rev. Lett. **77**, 3865 (1996).
[25] N. Troullier and J. L. Martins, Phys. Rev. B **43**, 1993 (1991).
[26] G. Kresse and J. Furthmuller, Comput. Mater. Sci. **6**, 15 (1996); Phys. Rev. B **54**, 11169 (1996).
[27] M. Y. Han, B. Özyilmaz, Y. Zhang, and P. Kim, Phys. Rev. Lett. **98**, 206805 (2007).
[28] L. Tapasztó, G. Dobrik, P. Lambin, and L. P. Biró, Nature Nanotech. **3**, 397 (2008).
[29] L. Weng, L. Zhang, Y. P. Chen, and L. P. Rokhinson, Appl. Phys. Lett. **93**, 093107 (2008).
[30] P. Nemes-Incze, G. Magda, K. Kamarás, and L. P. Biró, Nano. Res. **3**, 110 (2010).
[31] L. P. Biró and P. Lambin, Carbon **48**, 2677 (2010).
[32] P. Y. Huang, C. S. Ruiz-Vargas, A. M. van der Zande, W. S. Whitney, M. P. Levendor, J. W. Kevek, S. Garg, J. S. Alden, C. J. Hustedt, Y. Zhu, J. Park, P. L. McEuen, and D. A. Muller, Nature (London) **469**, 389 (2011).
[33] D. Gunlycke and C. T. White, Phys. Rev. Lett. **106**, 136806 (2011).
[34] O. V. Yazyev and S. G. Louie, Phys. Rev. B **81**, 195420 (2010).
[35] H. Lee, Y.-W. Son, N. Park, S. Han, and J. Yu, Phys. Rev. B **72**, 174431 (2005).
[36] L. Pisani, J. A. Chan, B. Montanari, and N. M. Harrison, Phys. Rev. B **75**, 064418 (2007).
[37] J. P. Perdew and Y. Wang, Phys. Rev. B **45**, 13244 (1992).
[38] R. M. Martin, *Electronic Structure, Basic Theory and Practical Methods* (Cambridge University Press, Cambridge, 2004), p.157.